Micromechanics of Fatigue Damage in Unidirectional Polymer Composites

Conference Paper *in* Collection of Technical Papers - AIAA/ASME/ASCE/AHS/ASC Structures, Structural Dynamics and Materials Conference · April 2012

DOI: 10.2514/6.2012-1650

4 authors, including:

Ray S Fertig III
University of Wyoming
55 PUBLICATIONS **259** CITATIONS

Micromechanics of Fatigue Damage in Unidirectional Polymer Composites

Mark R. Garnich[1], Ray S. Fertig III[2], Evan M. Anderson[3], Shiguang Deng[4]
University of Wyoming, Laramie, Wyoming, 82071

A work in progress is described that so far includes a finite element (FE) micromechanics modeling capability that generates random distributions of fibers in a periodic unit cell to predict fatigue damage in the matrix. The FE micromechanics model has automated features that facilitate parametric studies. This includes the ability to simulate any three-dimensional macroscopically uniform state of stress and to generate new fiber distributions within random-periodic unit cells that can have variable numbers of fibers. A damage evolution variable driven by the kinetic theory of fracture was implemented numerically in the FE computations. The spatial evolution of damage in the micromechanics model causes the deformation at some point to become unstable and define macroscopic failure of the composite. The effects of element size, time increment size, failed element residual properties, and fiber distribution were explored.

Nomenclature

h	=	Planck's constant
k	=	Boltzmann constant
K_b	=	molecular bond rupture rate
T	=	absolute temperature
U	=	activation energy
γ	=	activation volume
σ	=	effective stress
σ_1, σ_2, σ_3	=	ordered principal stresses
ξ	=	hydrostatic stress
η	=	second deviatoric stress invariant
ξ_0, η_∞	=	constants in isotropic failure criterion
ξ_p, η_p	=	stress point coordinates
ξ_f, η_f	=	stress point coordinates on failure surface
θ	=	orientation in the pi-plane

I. Introduction

FATIGUE failure analysis of polymer composites is of great importance to the continued advancement of such materials in structural applications. Previous modeling work has been dominantly empirical where experimental data for a particular material is used to calibrate mathematical functions that estimate fatigue life. As such, the models typically have a narrow application in terms of load history, stress state, and environmental conditions such as temperature and moisture. There is also a lack of modeling work that addresses the large scatter observed in polymer composite fatigue data.

The work described here is part of the early stages of a fundamental study of fatigue based on an idea proposed by Fertig and Kenik [1]. The basic premise of their work is that all composite damage initiates in the individual constituent materials within a composite and that multicontinuum theory (MCT) [2-3] provides a computationally efficient means of obtaining relevant constituent specific information about the state of stress. Furthermore, it is assumed that based on constituent stresses that the temporal evolution of damage can be captured within the matrix

[1] Associate Professor, Mechanical Engineering, 1000 E. University Ave., Laramie, WY, 82071, AIAA Member.
[2] Assistant Professor, Mechanical Engineering, 1000 E. University Ave., Laramie, WY, 82071, AIAA Member.
[3] Graduate Student, Mechanical Engineering, 1000 E. University Ave., Laramie, WY, 82071.
[4] Graduate Student, Mechanical Engineering, 1000 E. University Ave., Laramie, WY, 82071.

using the kinetic theory of fracture (KTF) [4]. The KTF embodies fundamental material constants including activation energy (U), activation volume (γ), and temperature (T) along with an effective stress (σ) to predict a molecular bond rupture rate (K_b). A basic form of the KTF equation is:

$$K_b = \frac{kT}{h}\mathbf{exp}\left(-\frac{U-\gamma\sigma}{kT}\right) \tag{1}$$

In the above, k is the Boltzmann constant and h is Planck's constant. As previously stated, Fertig applied this idea to the composite and utilized MCT to obtain constituent stress information as the basis for an effective stress for KTF calculations. Here we explore the application of KTF directly to the micro-stress field in the matrix as predicted by finite element (FE) micromechanics using Abaqus® [5]. Study of fatigue at the micro-stress level will help to understand how to formulate an effective stress based on the continuum stresses provided by MCT. Micromechanics of random fiber distributions will also permit study of the effect of fiber distribution on fatigue damage evolution and fatigue life.

The micromechanical model employed allows for either uniform hexagonal fiber packing or a "random-periodic" fiber packing as shown in Fig. 1. In both versions of the model the edges are subject to periodic boundary conditions so that the represented region of fiber and matrix behaves as though embedded in an infinite expanse repeating unit cells. Random fiber distributions are generated from initial uniform hexagonal arrays of fibers that are moved randomly and repeatedly so as to prevent overlap and to maintain a prescribed fiber volume fraction and periodic geometry as described in detail by Anderson [6]. The boundaries of the unit cell are based on the Voronoi cell concept [6] so that whole fibers are retained and the geometry is amenable to meshing with quadrilateral elements. A model is defined by specifying the number of fibers, the volume fraction of fiber, the number of times each fiber is to be randomly moved starting from the original hexagonal array, and the magnitudes of the macroscopic tensor stress components defining the state of stress to be simulated. The element size is controlled by specifying the number of elements around the circumference of each fiber. Linear elastic fiber properties (glass) were applied for all models in this study. Matrix material behavior was controlled using an Abaqus user subroutine (UMAT) [5].

A polymer failure criterion developed by Altenbach and Tushtev [7] was used to predict failure in the matrix elements of the micromechanics models. The criterion can be described in terms of the 3 ordered principal stresses ($\sigma_1 \geq \sigma_2 \geq \sigma_3$) using the concepts of deviatoric and hydrostatic stresses. Choosing the location of the pi-plane along the hydrostatic stress axis (ξ), the radial distance in the plane to the stress point (η), and the orientation in the plane (θ), we can write:

$$\xi = \frac{1}{\sqrt{3}}\left(\sigma_1+\sigma_2+\sigma_3\right) \tag{2}$$

$$\eta = \pm\frac{1}{\sqrt{3}}\sqrt{\left(\sigma_1-\sigma_2\right)+\left(\sigma_2-\sigma_3\right)+\left(\sigma_3-\sigma_1\right)} \tag{3}$$

$$\mathbf{tan}(\theta) = \frac{2\sigma_2-\sigma_1-\sigma_3}{\sqrt{3}\left(\sigma_1-\sigma_3\right)} \tag{4}$$

Assuming the failure surface is axisymmetric about the ξ-axis in principle stress space then a purely stress based criterion can be written in terms of two stress parameters ξ and η. The criterion proposed by Altenbach and Tushtev [7] is

$$\frac{1+\mathbf{exp}\left(\frac{\xi}{\xi_0}-1\right)}{1-\mathbf{exp}\left(\frac{\xi}{\xi_0}-1\right)}\left(\frac{\eta}{\eta_\infty}\right)=1. \tag{5}$$

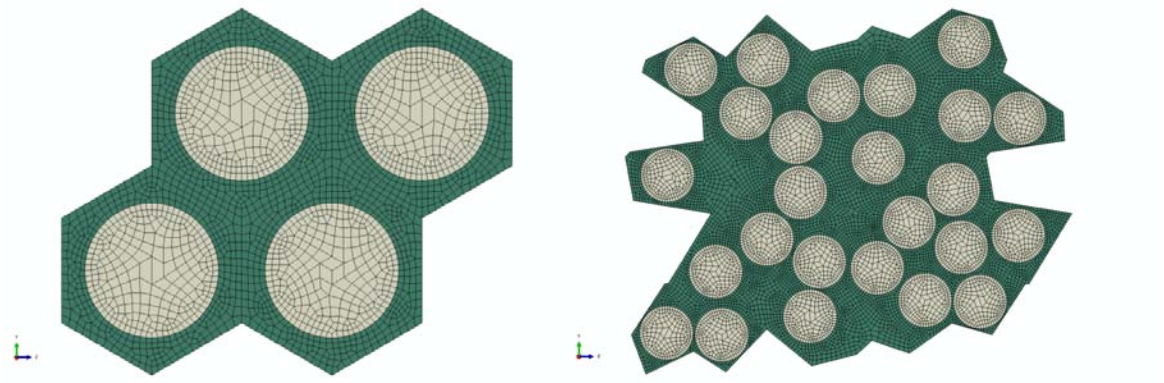

Figure 1. Hexagonal fiber packing FE micromechanics model (left) and random-periodic fiber packing model (right).

This convex failure surface is open in the direction of compressive hydrostatic stress. The parameters η_∞ and ξ_0 can be determined from the uniaxial tensile strength σ_t and uniaxial compression strength $-\sigma_c$. The axisymmetric failure surface can be depicted as a line on a plane of symmetry containing the hydrostatic stress axis **(ξ)** as shown in Fig. 2.

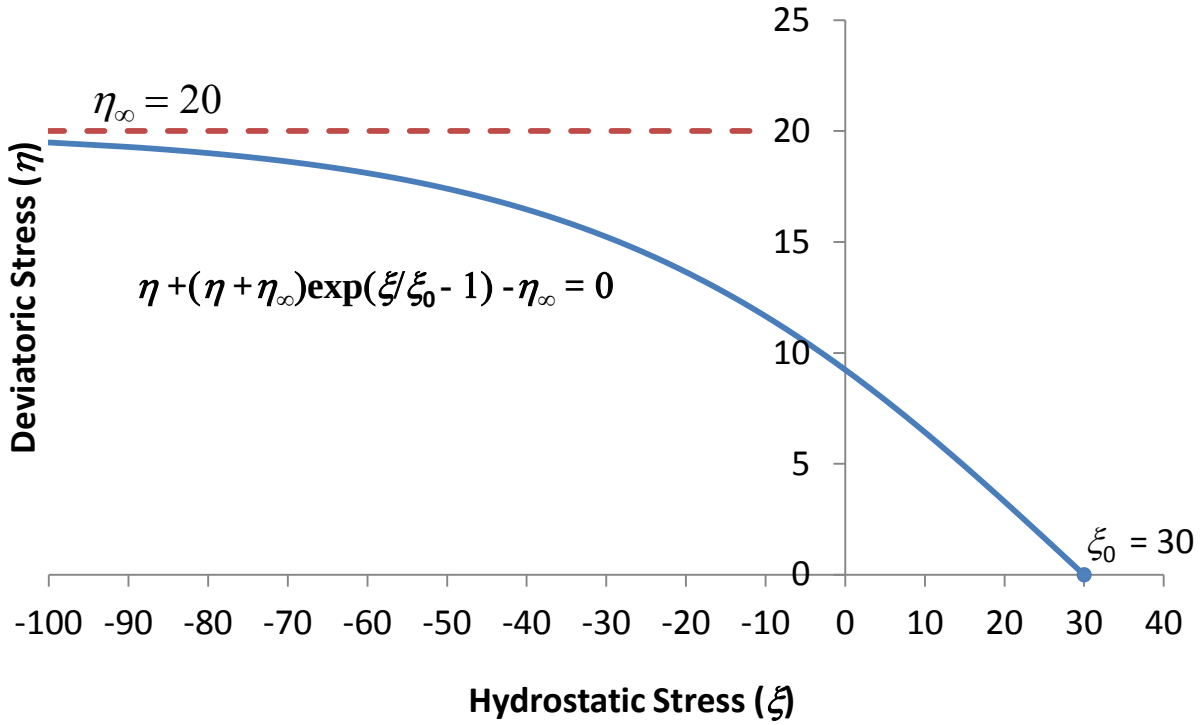

Figure 2. Polymer failure criterion represented in meridional plane ($\xi - \eta$ plane) assuming $\eta_\infty = 20$ and $\xi_0 = 30$.

II. Fatigue Failure Modeling

For fatigue calculations at the constituent level the matrix failure criterion can be used as a basis for employing the strength-life equal rank assumption [8-10]. This assumption states that if material samples could be tested for both static strength and fatigue life that each sample would have equal rank in the strength and life data sets for all

samples. Therefore, a static failure criterion can be used to rank components for fatigue life. Based on the polymer failure criterion depicted in Fig. 2 we define an effective stress that is assumed to drive the bond rupture rate modeled using the KTF. The portion of the failure surface for $0 < \xi < \xi_0$ is closely approximated by a cone. Thus, a slightly conservative approximation is given by the line $\frac{\eta}{\eta_\infty} = \frac{1-e^{-1}}{1+e^{-1}}\left(1-\frac{\xi}{\xi_0}\right)$, as shown by the dashed line in Fig. 3. For tensile hydrostatic stress (i.e. positive ξ_p) we assume the ratio of the distance from the origin to the point (ξ_p, η_p) to the distance from the origin to the point of intersection (ξ_p, η_p) on the same line with the failure surface is proportional to the effective stress for fatigue damage calculations. Assuming η_∞ is the maximum effective stress associated with any stress point (ξ_p, η_p), then the effective stress for any point with positive ξ is given by Eq. (6). Solving for η_f defined by the intersection of two lines shown in Fig. 4, and substituting into Eq. (6) gives Eq. (7).

$$\sigma = \frac{\eta_p}{\eta_f}\eta_\infty \text{ for } (\xi_p \geq 0) \tag{6}$$

$$\sigma = \left[\frac{1+e^{-1}}{1-e^{-1}}\left(\frac{\eta_p}{\eta_\infty}\right)+\frac{\xi_p}{\xi_\circ}\right]\eta_\infty \text{ for } (\xi_p \geq 0) \tag{7}$$

When the hydrostatic component of stress is negative the effective stress is assumed purely a function of the deviatoric component η_p. We choose the fraction of the associated deviatoric coordinate at failure, $\eta_f = \eta(\xi_p)$. That is, the effective stress is defined by Eq. (8) which gives some fraction of the stress η_∞ according to how close the state of stress is to the failure stress along the η coordinate on the deviatoric plane containing ξ_p. Substituting for η_f gives Eq. (9).

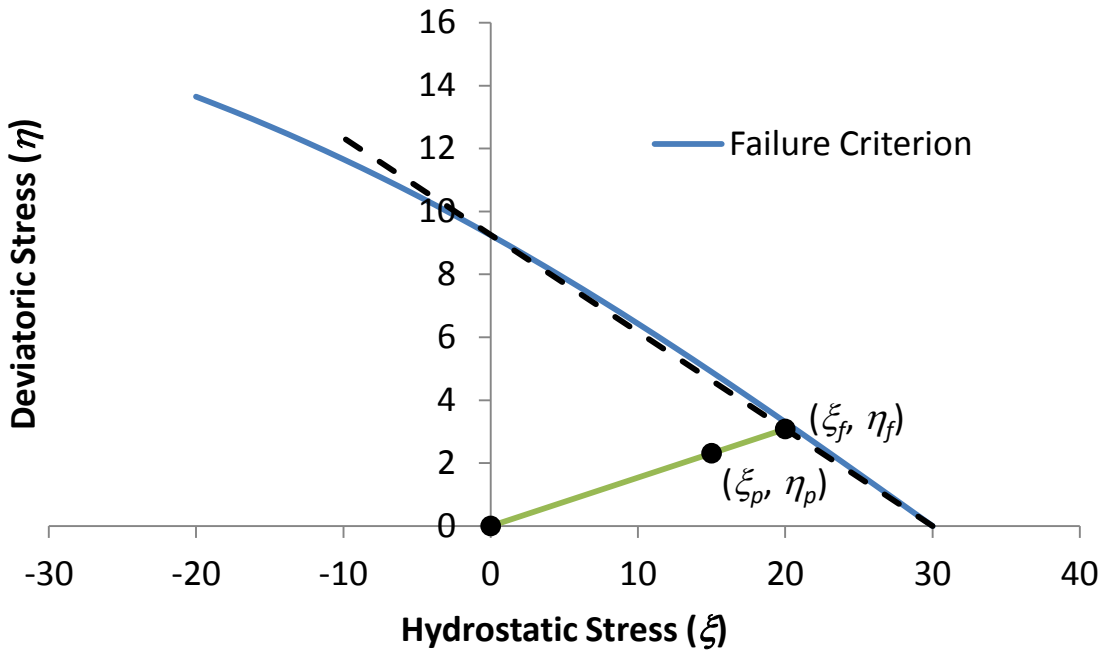

Figure 3. A linear approximation for the failure surface for positive ξ and arbitrary stress point (ξ_p, η_p) corresponding to point (ξ_f, η_f).

$$\sigma = \frac{\eta_p}{\eta_f(\xi_p)}\eta_\infty \text{ for } \left(\xi_p \le 0\right) \tag{8}$$

$$\sigma = \frac{1+\mathbf{exp}\left(\frac{\xi_p}{\xi_0}-1\right)}{1-\mathbf{exp}\left(\frac{\xi_p}{\xi_0}-1\right)}\eta_p \text{ for } \left(\xi_p \le 0\right) \tag{9}$$

Therefore, for any stress state defining a point $\left(\xi_p, \eta_p\right)$, the effective stress employed in Eq. (1) is defined by either Eq. (7) or (9) depending on whether the hydrostatic stress is positive or negative respectively. Note that Eq. (7) agrees with Eq. (9) when $\xi_p = 0$.

To complete the implementation of Eq. (1), an activation energy (U) and activation volume (γ) are required. The present modeling capability is in the development stages and at this point values were selected to be the same order of magnitude as applied by Hansen and Baker-Jarvis [11]. To model the effects of Eq. (1) in the matrix for FE models of the type shown in Fig. 1 a damage parameter (n) was defined following Fertig and Kenik [1] where initially there is no fatigue damage and $n = 0$. The evolution of n is defined by Eq. (10) where λ is a damage accumulation exponent (it was assumed here that $\lambda = 1$), K_b is defined by Eq. (1), and n_0 is a parameter that forces Eq. (10) to the creep solution under constant load. The magnitude of n_0 is determined by Eq. (11).

$$\frac{dn}{dt} = \left(n_0 - n\right)^\lambda K_b, \quad n(0) = 0 \tag{10}$$

$$\int_0^1 \frac{dn}{\left(n_0 - n\right)^\lambda} = 1 \tag{11}$$

In the FE computations that follow, damage is a discrete event that occurs when $n = 1$. The material retains the original linear elastic properties while $n < 1$ and is immediately degraded to some fraction of the original modulus when $n = 1$. The models are composed of 8-node brick elements with reduced (single point) integration. There are two state variables defined in the analyses. One state variable (SDV1) records the damage parameter n for each element and the second (SDV2) records the number of cycles when failure occurs (n becomes 1.0). Prior to failure, SDV2 = -1. In each increment a fixed number of load cycles are assumed to occur. For example, most of the results that follow were generated by specifying 100 increments with 10,000 cycles per increment for a total of 1,000,000 cycles. Therefore, SDV2 was only resolved to within 1% increments of the total load history.

III. Fatigue Modeling Results

To study the effects of some basic model parameters a hexagonal fiber array was initially assumed as shown in Fig. 1 (left). In what follows, "complete failure" is defined by occurrence of a path of failed matrix elements that connects opposite boundaries of the unit cell.

The FE models were generated automatically where the number of elements around the circumference of each fiber is specified to control the mesh density. Figure 4 shows two different mesh densities and the distribution of failed elements (SDV2) for the time of complete failure where it is seen that the damage patterns and cycles to failure (SDV2) are similar between the two models. In this and subsequent figures, blue elements are un-failed elements (SDV2 = -1) while other colors correspond the increment number or number of cycles at which the element failed. The models in Fig. 4 simulated a state of macroscopically uniform transverse tension. The issue of element size as related to progressive failure analysis is complex. This is not addressed here. Instead, the mesh was fixed with 96 elements around each fiber as in Fig. 4 on the right, so that the effect of other parameters could be considered independently.

For example, Fig. 5 shows several modeling results where the step increment size is varied with all other model parameters fixed. Again, the results are for transverse tension and are shown for the increment when complete failure occurs. Small numbers of increments (large step size) result in poor representation of the stress history. One affect of this is that the stress relief for some elements due to early failure of adjacent elements is not captured by the damage model. This causes a diffuse failure pattern where too many elements fail. From these results, it is shown that there are changes to the predicted distribution of damage for all changes in increment size down to the smallest increment size (5000 cycles per increment). However, the predicted time of complete failure is the same as for 10,000 cycles per increment. Therefore, to keep the computational expense reasonable, increments of 10,000 cycles were used in subsequent analyses. As will be seen, complete failure generally occurred somewhere between $6x10^5$ cycles and $7\ x10^5$ cycles depending on the fiber distribution and the specifics of the effective stress calculations.

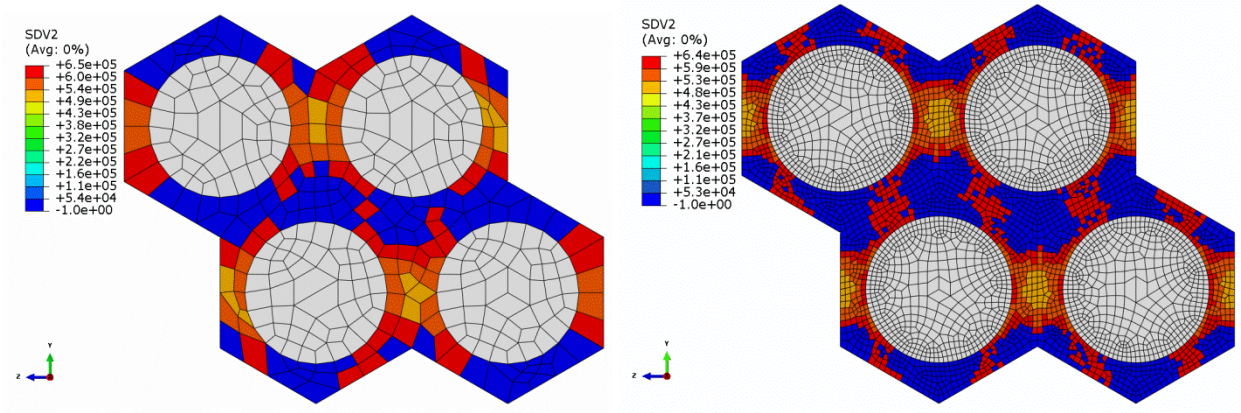

Figure 4. A comparison model results for two different meshes; 24 elements on a fiber circumference (left) and 96 elements on a fiber circumference (right).

It was noted that the failure criterion (Fig. 2) used as a basis for defining an effective stress (Eq. (7) and (9)) would give different results for tension and compression while, for example, a criterion based solely on the deviatoric stress (e.g. von Mises) would not. To verify this in the models would help to verify the numerical implementation of the effective stress. To do this, the von Mises stress was substituted as an effective stress and transverse uniaxial tension and compression tests were simulated. As expected, the results, in terms of fatigue life and damage distribution were the same for tension and compression when using von Mises stress as an effective stress. In contrast, changing from tension to compression load cases where Eq. (7) and (9) define the effective stress (σ) resulted in approximately a factor of 2 increase in predicted fatigue life.

Having confirmed basic qualitative behaviors of the modeling approach and established a reasonable element density and analysis increment size, random distributions of fibers were then modeled. Recall, these models are also periodic where the randomly distributed group of elements becomes the periodic unit cell. An example of results for a random distribution of 16 fibers is shown in Fig. 6 where the same fiber distribution was modeled three times. In the first model, failed elements were assigned degraded properties of 10% of the original elastic properties. In the second model they were assigned 1% of the original properties and in the third they were assigned 0.1% of the original properties. Leaving too much residual stiffness in the failed matrix elements causes too much load to be transmitted through them to adjacent elements which results in erroneous additional fatigue damage and eventual failure to occur in those elements. As seen in Fig. 6, the damage is quite diffuse when significant stiffness is retained in failed elements. Degrading failed element stiffnesses to near zero (0.1%) results in more realistic crack-like ribbons of failure propagating through the models.

The low residual stiffness also resulted in faster crack propagation so that complete failure of the unit cell occurred at about $6.1\ x10^5$ compared to $6.6\ x10^5$ cycles for the 1% residual stiffness and $7.5\ x10^5$ cycles for the 10% residual stiffness cases. This low stiffness had the additional pragmatic benefit of causing the Abaqus job to fail when complete failure was reached. This eliminated useless computations beyond failure of the unit cell while still allowing access to output data up to the point of Abaqus job failure. Subsequent models applied a 0.1% residual stiffness to failed matrix elements.

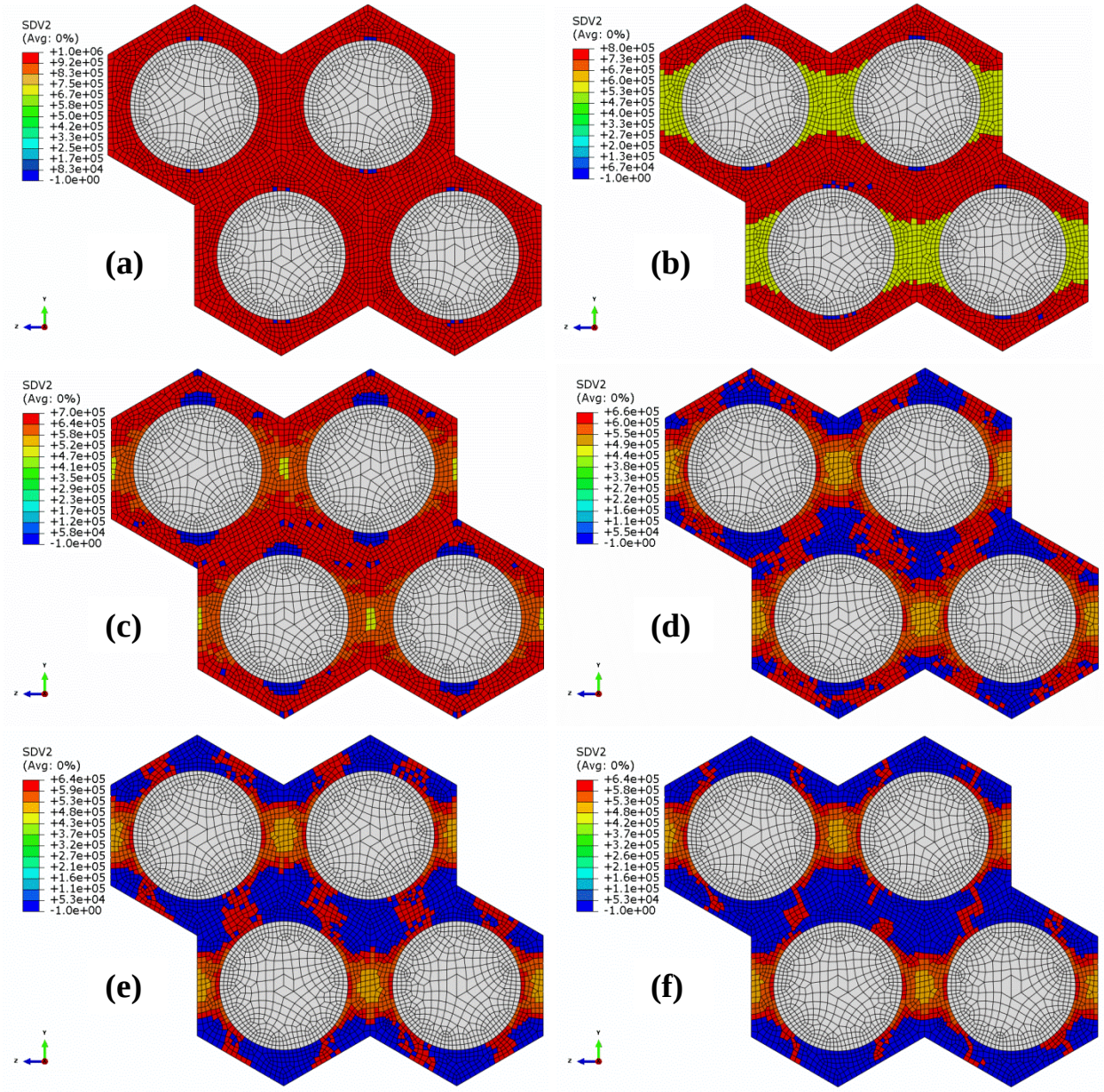

Figure 5. A comparison model results for six different increment sizes; (a) 1 increment = 10^6 cycles, (b) 5 increments = $2x10^5$ cycles/increment, (c) 10 increments = 10^5 cycles/increment, (d) 50 increments = 2x104 cycles per increment, (e) 100 increments = 10^4 cycles per increment, and (f) 200 increments = $5x10^3$ cycles per increment.

Finally, a series of 30 models were run where only the fiber distribution was changed in each. In all 30 models the fiber volume fraction was 50% and the increment step size was $1x10^4$ cycles. Using a residual element stiffness of 0.1% caused each of the Abaqus computations to fail at the increment where complete failure of the unit cell occurred. The number of load cycles at failure was recorded for each model. The results are summarized in Fig. 7 where the number of fiber distributions (models) that failed at each discrete increment in cycle number is shown. The mean is 635,000 cycles and the standard deviation is 14,000 cycles. This is a small standard deviation considering there is often one to two orders of magnitude scatter in composite fatigue data. This suggests that microscopic fiber distribution is a relatively minor contributor to observed overall variability in fatigue data.

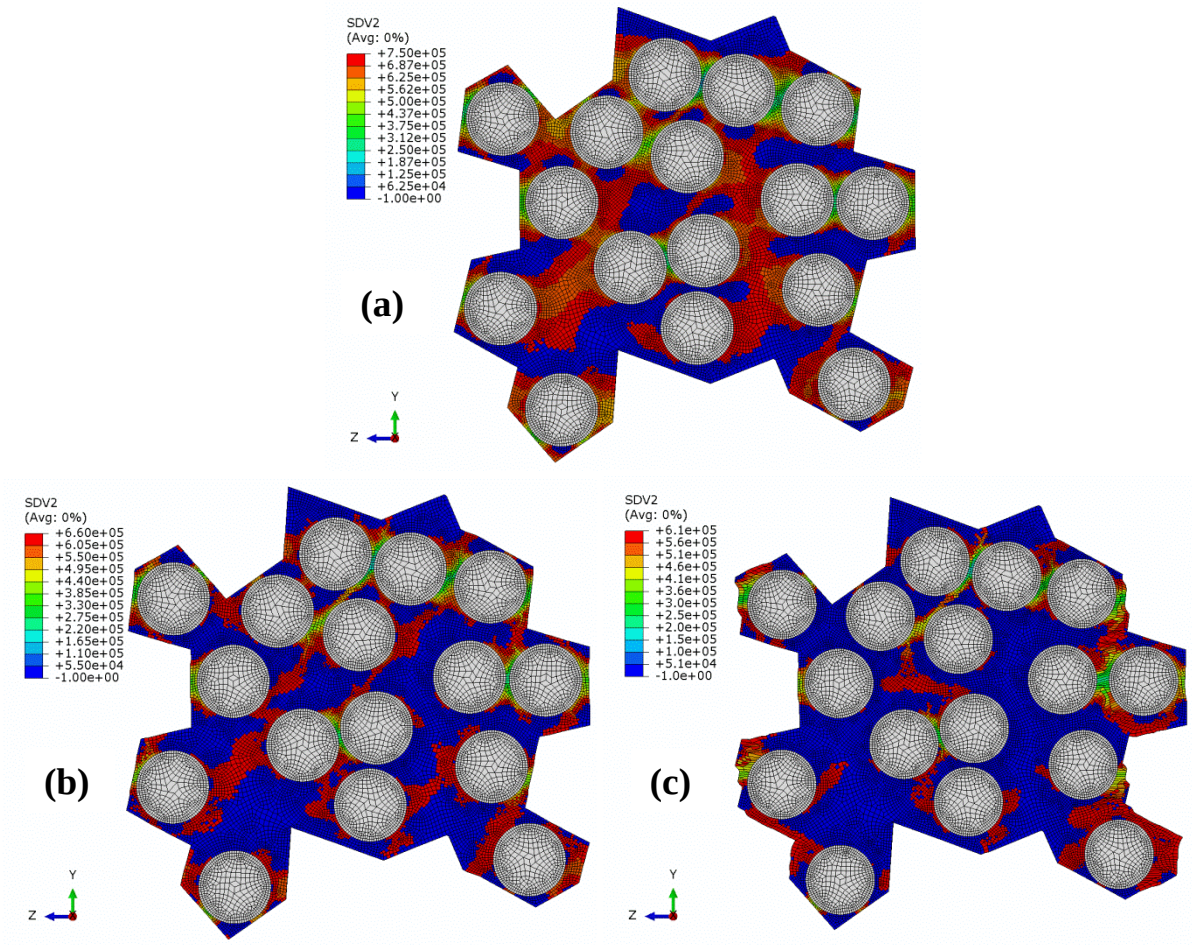

Figure 6. Fatigue damage distributions (blue is undamaged) at complete failure of the unit cell for different residual stiffness of failed elements; (a) 10%, (b) 1%, (c) 0.1% residual stiffness.

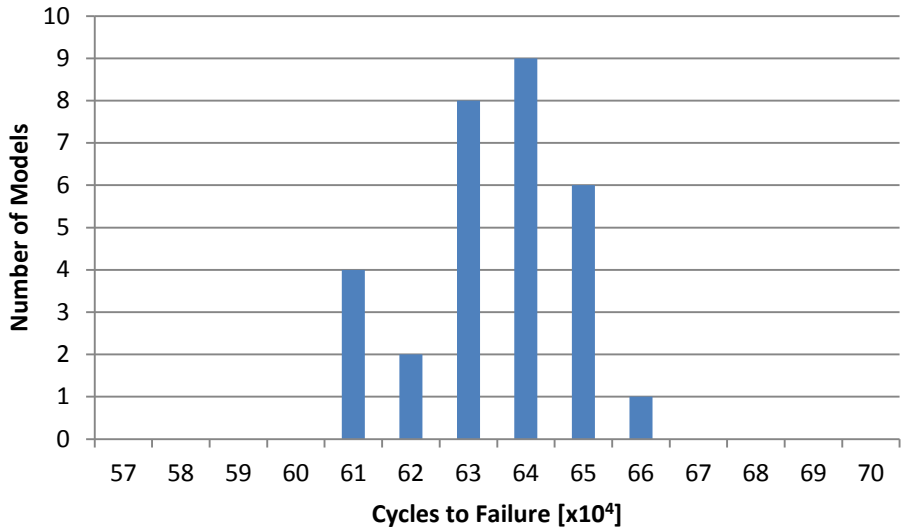

Figure 7. Predicted fatigue cycles to failure of 30 different unit cell models containing different random distributions of 16 fibers subject to transverse tension.

III. Conclusion

A finite element micromechanics modeling methodology has been described for study of fatigue failure in unidirectional fiber reinforced composites. The FE models are automatically generated for variable fiber volume fraction, number of fibers, element density, and macroscopic stress state. In addition, either uniform (hexagonal) or random fiber arrangements can be easily modeled. The models are three-dimensional, employing 8-node solid elements with reduced (single point) integration. The fiber materials were assumed linear elastic while a user material was defined in Abaqus to implement damage calculations for the matrix. Fatigue damage in the polymer matrix was assumed to be governed by the kinetic theory of fracture (KFT) where a rate of molecular disbonds is predicted and related to a continuously varying damage variable. The KTF provides a framework for employing physics of environment such as stress, temperature, and moisture in the predicting fatigue damage accumulation. In the present study only stress was introduced. An effective stress was defined based on the strength-life equal rank assumption [8-10] and a polymer failure criterion [7] that accounts for hydrostatic tension versus compression effects on failure. In the micromechanics models failure was accounted for as a discrete event occurring when the damage variable reached a critical value. At that point the element properties were instantaneously degraded to some fraction of the original elastic properties.

A number of computational experiments were conducted. Complete failure was defined as when a path of failed matrix elements spanned the model. It was shown that an element density corresponding to about 100 elements around a fiber circumference and a step size on the order of 1% of the total time or cycles to complete failure was adequate to capture the time varying distribution of damage and the time of complete failure. It was also shown that the residual stiffness of failed elements needed to be less than 1% of the original stiffness to obtain the most realistic spatial distributions of failed elements. Finally, a group of 30 simulations was conducted varying only the fiber distribution in a 16 fiber model. The results gave a standard deviation of about 2% of the mean value, indicating that the randomness fiber distribution may only account for a small portion of the scatter in composite fatigue data.

The modeling work described here is just the initial stage of this effort. Future work will include a various parametric studies such as multiaxial stress states, number of fibers in the unit cell, fiber volume fraction, residual stress, and element size. The issue of touching or nearly touching fibers and the nature of failure between these fibers will be studied. Cohesive zone modeling will be implemented at the fiber-matrix interface so that the effect of competing failure modes; interface versus matrix failure can be studied. Also, the present micromechanics model has the capability for specifying a fiber waviness where a three dimensional volume is extruded in the fiber direction while still automatically generating periodic boundary conditions and general macroscopic equivalent stress states. Application of this capability will allow study of effects of fiber waviness on fatigue failure.

Acknowledgment

The authors would like to acknowledge support through a gift from BP Alternative Energy North America Inc.

References

[1]Fertig, R. S. and Kenik, D. J., Predicting Composite Fatigue Life Using Constituent-Level Physics," *52nd AIAA/ASCE/AHS/ASC Structures, Structural Dynamics, and Materials Conference Proceedings*, AIAA 2011, Denver, Colorado, April 2011.

[2]Garnich, M. R. and Hansen, A. C., "A Multicontinuum Approach to Structural Analysis of Linear Viscoelastic Composite Materials," *Journal of Applied Mechanics*, Vol. 64, No. 4, 1997, pp.795-803.

[3]Garnich, M. R. and Hansen, A. C., "A Multicontinuum Theory for Thermal-Elastic Finite Element Analysis of Composite Materials," *Journal of Composite Materials*, Vol. 31, No. 1, 1997, pp.71-86.

[4]Zhurkov, S. N., "Kinetic Concept of the Strength of Solids," *International Journal of* Fracture, Vol. 26, 1984, pp. 295-307.

[5]Abaqus, Version 6.10, Dassault Systèmes Simulia Corp., 2010, 166 Valley Street, Providence, RI 02909.

[6]Anderson, E. M., "An Automated Finite Element Program for Micromechanics Modeling of Random-Wavy Fiber Composites," M.S. Thesis, Dept. of Mechanical Engineering, Univ. of Wyoming, Laramie, WY, 2010.

[7]Altenbach, H. and Tushtev. K., "A New Static Failure Criterion for Isotropic Polymers," *Mechanics of Composite Materials*, Vol. 37, No. 5/6, 2001, pp. 475-482.

[8]Hahn, H. T. and Kim, R. Y., "Proof Testing of Composite Materials," *Journal of Composite Materials*, Vol. 9, 1975, pp. 297-311.

[9]Chou, P. C. and Croman, R., "Residual Strength in Fatigue Based on the Strength-Life Equal Rank Assumption," *Journal of Composite Materials*, Vol. 12, 1978, pp. 177-194.

[10]Barnard, P. M., Butler, R. J., and Curtis, P. T., "The Strength-Life Equal Rank Assumption and its Application to Fatigue Life Prediction of Composite Materials," *International Journal of Fatigue*, Vol. 10, No. 3, 1988, pp. 171-177.

[11]Hansen, A. C. and Baker-Jarvis, J., "A rate dependent kinetic theory of fracture for polymers," *International Journal of Fracture* Vol. 44, 1990, p. 221-231.